Journal of Alloys and Compounds, 209 (1994) 351–361
JALCOM 1119

A mathematical and experimental dynamical phase diagram for ball-milled $Ni_{10}Zr_7$

M. Abdellaoui* and E. Gaffet*,**

CNRS, UPR, AO423, "Far From Equilibrium Phase Transition Group", Institut Polytechnique de Sevenans, F-90010 Belfort Cedex (France)

(Received October 22, 1993; in final form January 14, 1994)

Abstract

Based on a deeper mathematical treatment of the process taking place in a planetary ball mill and experimental results concerning the ball-milled end product of the $Ni_{10}Zr_7$ compound, we prove that neither the shock frequency nor the shock energy separately governs the ball-milled end product as assumed previously. In other words, we prove that the ball-milled end product is only governed by the shock power.

Based on these calculated and experimental results, a ball-milled dynamic phase diagram is mapped into three regions: a pure amorphous phase for medium shock power values ranging from 4 to 8.2 W (corresponding to 0.4–0.82 W g^{-1} for 10 g $Ni_{10}Zr_7$ powder mass); a mixture of crystalline and amorphous phases for low (less than 4 W) and high (greater than 8.2 W) shock power values.

1. Introduction

By ball milling pure elements as well as intermetallic compounds, we induce an energy transfer from the milling tools to the milled powders. The results of such a milling process are various. We can achieve the formation of amorphous phases by milling pure elements [1–3] or elemental metal ribbons [4, 5] and the formation of intermetallics from pure elements [6, 7]. Also, mechanical alloying (MA) is a process used for producing powders with a fine microstructural scale [8] and/or a technique for alloying immiscible materials [9]. A solid solution can also be considerably supersaturated compared with the thermodynamic equilibrium [10]. The process is also inherently flexible. However, there has been little attempt to analyse it in a manner that would establish predictive capabilities for it. Thus, up to now, apart from a few scattered results, no attempt has been made to obtain a precise description of this complex process.

In fact, Burgio *et al.* [11] attempt to correlate the milling operative conditions and the end product in a Fritsch "Pulverisette P5" ball mill. The authors try to study the influence of the ball radius, ball mass and number of balls used on the end product. By a geometrical method they try to find the condition of a first collision event after the first detachment for given disc and vial rotation speeds in order to evaluate the kinetic energy released to the powders during the collision event.

Maurice and Courtney [12] try to give an approach defining the geometry and the basic mechanics of the powder–ball interaction for several common devices used for MA, since such information allows pertinent parameters of the process (*e.g.* impact velocity, powder material volume impacted, time between impacts, etc.) to be identified in terms of machine characteristics and process operating parameters.

In both the above-mentioned works [11, 12] the shock energy and ball-milling duration were assumed to be the only parameters governing the ball-milling process.

Thus, based on the results of a deeper mathematical treatment of the process taking place in a planetary ball mill and experimental results on the ball-milled end product of the $Ni_{10}Zr_7$ compound, the purpose of this paper is to prove that neither the shock energy nor the shock frequency separately can govern the end product. In other words, we prove that the end product depends only on the shock power, which is the product of the shock energy and shock frequency.

2. Numerical calculation results

Our calculations are carried out for two different planetary ball mills called G5 and G7. The so-called

*Former address: ISITEM, CNRS, "Far From Equilibrium Phase Transitions Group", La Chantrerie, Rue C. Pauc, CP3023, F-44087 Nantes Cedex 03, France.

**Author to whom correspondence should be addressed.

0925-8388/94/$07.00
SSDI 0925-8388(94)01119-3

G5 and G7 planetary ball mills exhibit the same disc radii as the so-called Fritsch "Pulverisette 5" and "Pulverisette 7" respectively. The aims of the construction of these two devices are (i) the possibility of varying the disc and vial rotation speeds independently and (ii) the study of the disc radius effect on the kinetic energy, shock frequency and shock power. Furthermore, an ultrasonic tachometer control during the milling process allows effective control of the vial and disc rotation speeds.

The disc radiis corresponding to the G5 and G7 planetary ball mills are 132×10^{-3} and 75×10^{-3} m respectively. The vial radius is 21×10^{-3} m. The ball radius and ball mass are 7.5×10^{-3} m and 14 g respectively. Five balls are used in order to calculate the shock energy, shock frequency and shock power.

Figures 1–3 (full curves, G5 mill; dashed curves, G7 mill) show the kinetic energy released from one ball to the powders in one hit, the shock frequency and the shock power respectively as a function of the disc and vial rotation speeds. The details of these calculated results are given in the Appendix.

Based on these figures, the kinetic energy and shock power increase as a function of the disc and vial rotation speeds. The shock frequency decreases for disc rotation speeds ranging from 0 up to 250 rev min^{-1} and then increases almost linearly as the disc rotation speed increases further.

For the G5 planetary ball mill the maximum kinetic energy can reach 0.9 J per hit (0.3 J per hit for the

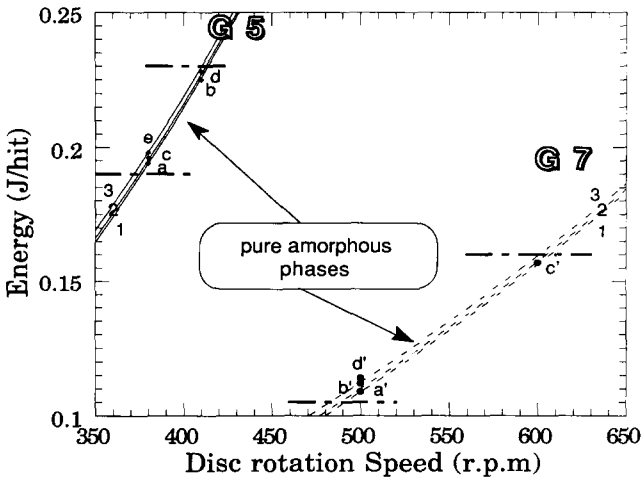

Fig. 1. Kinetic energy imparted by one hit as a function of disc and vial rotation speeds corresponding to G5 (full curves) and G7 (dashed curves) planetary ball mills. The vial rotation speed values are indicated by the numbers 1–3 written near each corresponding curve: 1, 150 rev min^{-1}; 2, 250 rev min^{-1}; 3, 350 rev min^{-1}. The kinetic energies corresponding to the experimental ball-milling conditions, illustrated in Fig. 4 by the data points a, b, c, d and e for the G5 device and a', b', c' and d' for the G7 device, leading to the same pure amorphous phase formation are reported.

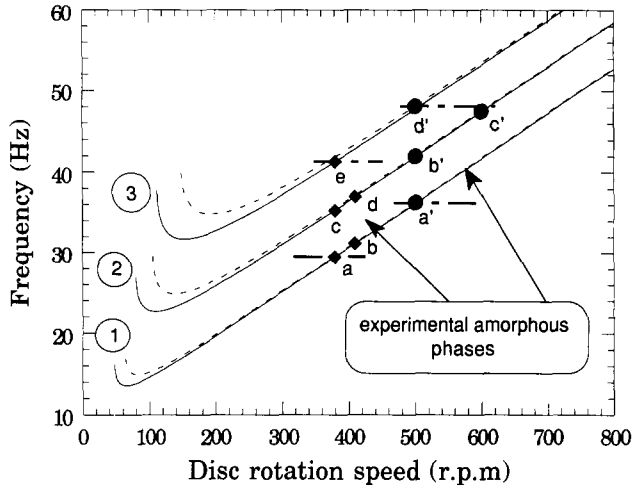

Fig. 2. Shock frequency as a function of disc and vial rotation speeds for G5 (full curves) and G7 (dashed curves) planetary ball mills. The vial rotation speed values are indicated by the numbers 1–3 written near each corresponding curve: 1, 150 rev min^{-1}; 2, 250 rev min^{-1}; 3, 150 rev min^{-1}. The shock frequencies corresponding to the experimental ball-milling conditions, illustrated in Fig. 4 by the data points a, b, c, d and e for the G5 device and a', b', c' and d' for the G7 device, leading to pure amorphous phase formation are reported.

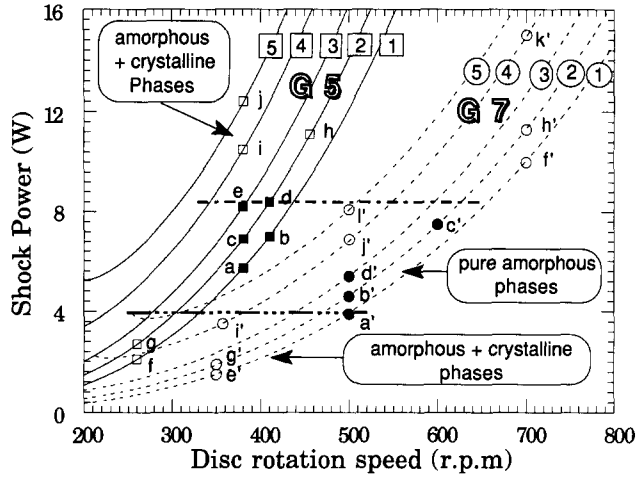

Fig. 3. Shock power as a function of disc and vial rotation speeds for G5 (full curves) and G7 (dashed curves) planetary ball mills. The vial rotation speed values are indicated by the numbers 1–5 written near each corresponding curve: 1, 150 rev min^{-1}; 2, 250 rev min^{-1}; 3, 350 rev min^{-1}; 4, 500 rev min^{-1}; 5, 600 rev min^{-1}. The shock powers corresponding to the experimental ball-milling conditions, illustrated in Fig. 4 by the data points a, b, c, d and e for the G5 device and a', b', c' and d' for the G7 device, leading to the same pure amorphous phase formation as well as the shock power values corresponding to the experimental ball-milling conditions, illustrated in Fig. 4 by the data points f, g, h, i and j for the G5 device and e', f', g', h', i', j', k' and l' for the G7 device, leading to the formation of a mixture of crystalline and amorphous phases are reported.

G7 device) for disc and vial rotation speeds of 800 rev min^{-1}. The shock frequency and shock power can reach 90.7 Hz (92.4 Hz for the G7 device) and 80.2 W (28 W for the G7 device) respectively for disc and vial rotation speeds of 800 rev min^{-1}.

3. Calculated and experimental results for the $Ni_{10}Zr_7$ compound ball-milled end product

Gaffet and Yousfi [13] have used the G5 and G7 ball-milling machines to study the effect of the ball-milling conditions on the end product in the $Ni_{10}Zr_7$ compound. In this work [13], 10 g of melt-spun ribbon pieces (dimensions about 8 mm×10 mm×50 μm) of mean composition $Ni_{58.8}Zr_{41.2}$ (in atomic per cent), corresponding to the $Ni_{10}Zr_7$ intermetallic compound, are introduced into a cylindrical tempered steel container of capacity 45 ml. This procedure is carried out in a glove-box filled with purified argon. Each container is loaded with five steel balls 1.5 cm in diameter and 14 g in mass. The containers are sealed in the glove-box with a Teflon O-ring and the milling proceeds in a stationary argon atmosphere. The ball-milling duration of the stationary state was 48 h. The structures of the as-prepared melt-spun ribbons have been checked by X-ray diffraction (XRD) patterns and have been confirmed to correspond purely to the $Ni_{10}Zr_7$ intermetallic compound. For the ball-milled samples a numerical method "ABFfit programme" was used in order to analyse the XRD patterns and to obtain the position and full width at half-height of the various peaks. The crystalline phases taken into account are those which correspond to the equilibrium phases in the Ni–Zr phase diagram. The amorphous phase compositions were determined using the previously established Vegard-type law $d = 7.79\times10^{-4}x + 0.1901$, where d is the position of the first amorphous halo (in nanometres) and x is the composition of the amorphous phase $Ni_{1-x}Zr_x$ (x is expressed in atomic per cent).

The authors [13] show that the formation of a pure amorphous phase is found when operating with the ball-milling conditions given in Table 1. In this table we report the experimental ball-milling conditions (ω, the vial rotation speed; Ω, the disc rotation speed), the calculated kinetic energy E_k, the calculated shock frequency f, the calculated shock power P and the calculated cumulative kinetic energy E_{kc} corresponding to the experimental data points a, b, c, d and e for the G5 planetary ball mill and a′, b′, c′ and d′ for the G7 planetary ball mill reported in Fig. 4. This figure shows a superimposition of the end product structure corresponding to the ball milling of the $Ni_{10}Zr_7$ compound at room temperature by means of the G5 and G7 machines. On the left-hand Y axis the Ω_{G7} rotation speeds are reported and on the right-hand Y axis the Ω_{G5} values. These have been chosen in order to agree with the equation $(\Omega_{G7})^2R_{G7} = (\Omega_{G5})^2R_{G5}$. The authors [13] assume that this equation expresses an approximate equivalent energy between the two different devices. Nevertheless, taking into account the assumption of Chen *et al.* [14] that the shock power injected into the powders by planetary ball milling scales with $m\ r\ R\ \Omega^2\ \omega$ (with m the ball mass, r and R the vial and disc radii respectively and Ω and ω the disc and vial rotation speeds respectively), the energy equivalence assumed by Gaffet and Yousfi [13] corresponds to a power equivalence as assumed by Chen *et al.* [14] when operating with the same vial radius, vial rotation speed and ball mass.

The same authors [13] report on the experimental ball-milling conditions leading to the formation of a

TABLE 1. Calculated kinetic energies, shock frequencies, shock powers and cumulative kinetic energies corresponding to the experimental ball-milling conditions, illustrated in Fig. 4 by the data points a, b, c, d and e for the G5 device and a′, b′, c′ and d′ for the G7 device, leading to the same pure amorphous phase formation

Experimental data point (Fig. 4)	ω (rev min^{-1})	Ω (rev min^{-1})	E_k (10^{-3} J per hit)	f (Hz)	P (W)	E_{kc} (kJ)
G5 planetary ball mill						
a	127	380	194	29.5	5.7	988
b	127	410	226	31.2	7.0	1215
c	250	380	195	35.3	6.9	1191
d	250	410	227	37.0	8.4	1448
e	350	380	198	41.3	8.2	1413
G7 planetary ball mill						
a′	127	500	109	36.3	3.9	682
b′	250	500	109	42.0	4.6	796
c′	250	600	157	47.5	7.5	1289
d′	350	500	112	48.1	5.4	931

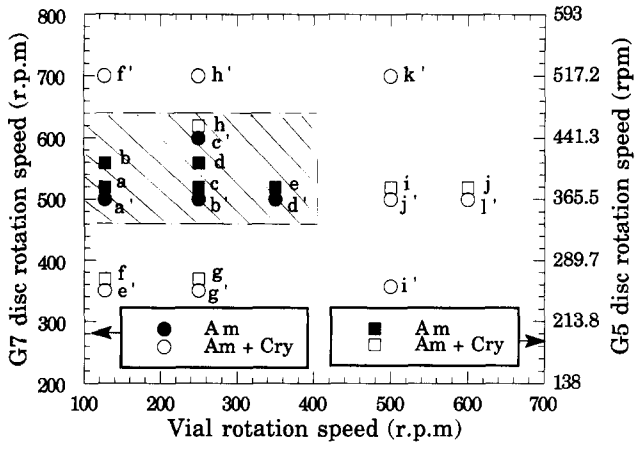

Fig. 4. Superimposition of end product structure corresponding to ball milling of the $Ni_{10}Zr_7$ compound at room temperature by means of G5 and G7 machines. On the left-hand Y axis the Ω_{G7} rotation speeds are reported and on the right-hand Y axis the Ω_{G5} values. The filled symbols correspond to pure amorphous phases, whereas the empty symbols correspond to a mixture of crystalline and amorphous phases. The hatched areas correspond to the two amorphous domains.

mixture of amorphous and crystalline phases. In Table 2 we report these experimental ball-milling conditions (ω, the vial rotation speed; Ω, the disc rotation speed) as well as the calculated kinetic energy E_k, the calculated shock frequency f, the calculated shock power P and the calculated cumulative kinetic energy E_{kc}. These experimental and calculated parameters correspond to the data points f, g, h, i and j for the G5 planetary ball mill and e', f', g', h', i', j', k' and l' for the G7 planetary ball mill reported in Fig. 4. Thus in Fig. 4 the hatched areas containing the filled symbols correspond to the two amorphous domains, whereas the empty symbols correspond to the mixture of crystalline and amorphous phases.

Eckert *et al.* [15] elaborate amorphous powders by mechanical alloying from Ni–Zr crystalline elemental powders. The mechanical alloying was performed in a conventional planetary ball mill (Fritsch "Pulverisette 5"). The ball-milling intensities used are 3, 5 and 7. The authors [15] show that for ball-milling intensity 5 a pure amorphous phase is formed from about 30 to 83 at.% Ni. The ball-milling duration required to achieve the amorphization process was 60 h. For ball-milling intensity 7, for the same ball-milling duration (60 h), the authors report the formation of an intermetallic phase from $x = 66$ to 75 at.% Ni. For ball-milling intensity 3 complete amorphization was not achieved for a ball-milling duration of 60 h.

In the present work we try to see how the kinetic energy, shock frequency and shock power affect the end product and to determine whether a correlation between one of these parameters and the end product can be systematically established. Thus it is first important to check whether there is an overlap between the kinetic energy domains corresponding to the same amorphous phases (as reported in Fig. 4). Based on our mathematical treatment of the process taking place in the planetary ball mill, we only report in Fig. 1 the calculated shock energies corresponding to the experimental ball milling conditions, illustrated in Fig. 4 by the data points a, b, c, d and e for the G5 device and a', b', c' and d' for the G7 device, leading to the same amorphous phase formation [13]. The calculated shock energies leading to amorphous phase formation for the

TABLE 2. Calculated kinetic energies, shock frequencies, shock powers and cumulative kinetic energies corresponding to the experimental ball-milling conditions, illustrated in Fig. 4 by the data points f, g, h, i and j for the G5 device and e', f', g', h', i', j', k' and l' for the G7 device, leading to the formation of a mixture of amorphous and crystalline phases

Experimental data point (Fig. 4)	ω (rev min^{-1})	Ω (rev min^{-1})	E_k (10^{-3} J per hit)	f (Hz)	P (W)	E_{kc} (kJ)
G5 planetary ball mill						
f	127	260	91	22.9	2.1	361
g	250	260	93	28.9	2.7	464
h	250	456	280	39.5	11.1	1909
i	500	380	206	50.8	10.5	1808
j	600	380	214	57.6	12.4	2132
G7 planetary ball mill						
e'	127	350	53	28.0	1.5	258
f'	127	700	212	47.3	10.0	1732
g'	250	350	55	34.0	1.9	322
h'	250	700	213	53.0	11.3	1951
i'	500	357	68	51.5	3.5	608
j'	500	500	118	57.7	6.9	1181
k'	500	700	220	68.0	15.0	2583
l'	600	500	125	64.7	8.1	1397

G5 device (circles) range from about 194×10^{-3} to about 227×10^{-3} J per hit. For the G7 ball mill (diamonds) the calculated shock energies leading to the same amorphous phases as the G 5 ball mill range from about 109×10^{-3} to about 157×10^{-3} J per hit.

As shown in Fig. 1, there is no overlap between the two energy domains corresponding to the same amorphous phase formation when using the G5 and G7 devices. If the kinetic energy was the unique parameter governing the amorphous phase formation, the same amorphous phases formed either by the G5 or by the G7 machine would correspond to the same kinetic energy irrespective of the mill's physical and kinematical characteristics. Since this condition is not fulfilled, this means that the one-hit kinetic energy separately cannot be a unique independent parameter governing the amorphous phase transition.

The calculated shock frequencies corresponding to the experimental ball-milling conditions, illustrated in Fig. 4 by the data points a, b, c, d and e for the G5 device and a', b', c' and d' for the G7 device, leading to amorphous phase formation are reported in Fig. 2. As concluded above for the shock energy, there is no perfect overlapping between the two frequency domains corresponding to the same amorphous phases formed when using the two different devices. Nevertheless, a narrow overlap may exist for the ball-milling conditions corresponding to the limit of the phase domains. Thus it is clear that the shock frequency and kinetic energy influence the end product structural state but cannot be considered as being independent parameters governing the ball-milled end product.

The calculated shock powers corresponding to the experimental ball-milling conditions, illustrated in Fig. 4 by the data points a, b, c, d and e for the G5 device and a', b', c' and d' for the G7 device, leading to amorphous phase formation are reported in Fig. 3. Based on this figure, there is nearly perfect overlapping between the shock power domains leading to the same amorphous phases formed when using the G5 (circles) and G7 (squares) devices. Moreover, when considering in Fig. 3 the calculated shock powers corresponding to the experimental ball milling conditions, illustrated in Fig. 4 by the data points f, g, h, i and j for the G5 device and e', f', g', h', i', j', k' and l' for the G7 device, leading to the formation of a mixture of crystalline and amorphous phases, we see that all the power values corresponding to these experimental data points lie outside the shock power domain corresponding to pure amorphous phase formation (bounded by the two horizontal chain lines). Thus we conclude that neither the shock energy nor the shock frequency separately governs the end product, but that only the injected shock power is responsible for the ball-milled end product.

Moreover, mechanical alloying differs from conventional mechanical straining tests (*i.e.* traction or compression tests) in its mechanical situation type. In fact, if conventional mechanical straining tests are static situations with continuous constant intensity with time, mechanical alloying can be considered simply as a dynamic cyclic mechanical situation constituted by repeated shocks of constant amplitude and frequency. In a first approximation it can be regarded as a fatigue test with repeated asymmetric stress as illustrated in Fig. 5(a).

It has been reported that b.c.c. (Fe, Cr, Nb, and W) and h.c.p. (Zr, Hf, Co, Ru) structural materials are easily obtained as nanostructural materials [16]. This is related to their high elastic energy storage ability. In fact, this stored elastic energy, when it exceeds a critical value, leads to an explosion of the particles and thus to grain size refinement. The latter can induce amorphous phase formation if the grain size becomes less than a critical value.

In conventional mechanical straining (*i.e.* traction or compression tests) the stored elastic energy per unit volume cell is only a function of the constant applied stress and the powder Young's modulus. It is given by the area over the rational traction curve as

$$W=\frac{1}{2}\frac{\sigma^2}{2Y} \tag{1}$$

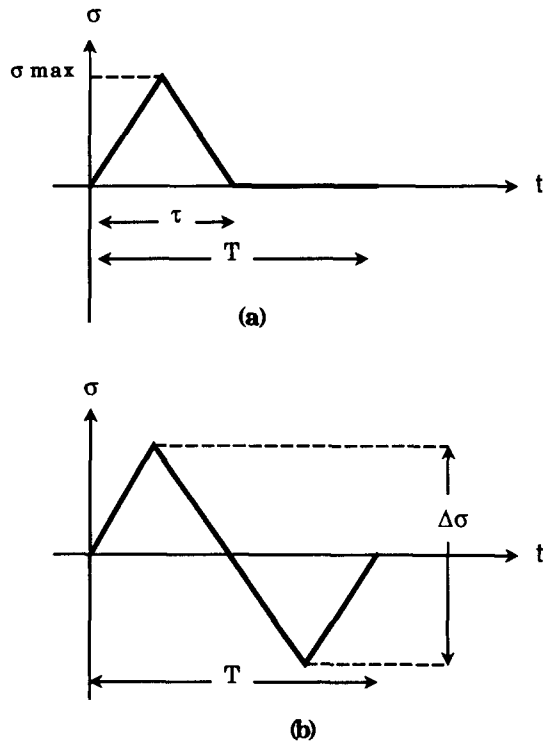

Fig. 5. Schematized stress variation in (a) the ball-milling process and (b) a symmetric altered stress conventional fatigue test.

In the conventional fatigue test with a symmetric altered stress (Fig. 5(b)) the rational curve presents a hysteresis shape. The stored elastic energy per unit volume cell will be given by the area of the hysteresis loop. In contrast, the stress in mechanical alloying cannot be negative and thus we cannot obtain a hysteresis loop. Based on Fig. 5, the stress can take the following form as a function of time:

$$\text{for } 0 < \frac{\tau}{2}, \qquad \sigma(t) = \frac{2}{\tau}\sigma_{\max} t \tag{2}$$

$$\text{for } \frac{\tau}{2} < t < \tau, \qquad \sigma(t) = -\frac{2}{\tau}\sigma_{\max} t + 2\sigma_{\max} \tag{3}$$

$$\text{for } t < t < T, \qquad \sigma(t) = 0 \tag{4}$$

with $\sigma_{\max}$ the maximum stress, τ the impact duration and T the shock cycle period. The calculation of the stored elastic energy per unit volume cell will be done for one period. The elemental stored elastic energy is given by $dW = \sigma\, d\epsilon$. Let us suppose in a first approximation that the stress σ can be expressed as $\sigma = Y\epsilon$. Thus the stored energy for one cycle is

$$W = \frac{1}{T}\int_0^{\tau} \frac{\sigma(t)}{Y}\, d\sigma \tag{5}$$

Taking into account eqns. (2)–(4), the stored elastic energy per unit volume cell is given by

$$W = \frac{1}{T}\frac{\sigma_{\max}^2}{Y} = f\frac{\sigma_{\max}^2}{Y} \tag{6}$$

The maximum stress $\sigma_{\max}$ expresses the maximum force $F_{\max}$ per unit surface developed during the impact. The maximum force expresses the ball kinetic energy per unit length. Thus it is easy to see by simple calculations that in contrast with the static situation (eqn. (1)), the stored elastic energy per unit volume cell in the case of mechanical alloying is a function of both the maximum stress, which expresses the ball kinetic energy, and the shock frequency. Therefore we show by these simple calculations that neither the shock energy nor the shock frequency separately governs the end product, but that only the injected shock power is responsible for the ball-milled end product.

It is well known that in the conventional steady state (depending only on the temperature and the concentrations of the various elements of the system) a structural phase transformation occurs only if the system free energy can step over the corresponding activation energy barrier. By analogy, we assume that in the mechanically alloyed state a structural phase transition occurs only if the defect creation rate steps over an activation defect creation rate. In simpler terms, we assume that the structural phase transition occurs only if the shock power (or the stored elastic energy per unit volume cell) steps over a shock power critical value.

Thus we assume that if the shock power is lower than a minimum value, mechanical alloying induces, after a long ball-milling duration, only a refinement of the powder grain size and an increase in the defect quantity until reaching a steady state which is not able to be destabilized into another structural state, whereas if the shock power is greater than a minimum power value, mechanical alloying induces a refinement of the powder grain size and an increase in the defect quantity at a rate able to induce, even in the earlier stages of mechanical alloying, a mixture of structurally transformed phase and initial phase. In the latter case the steady state can result, depending on the value of the shock power, in a mixture of structurally transformed phase and initial phase or in a homogeneous structurally transformed phase. The steady state is reached when elastic energy storage in the powders becomes impossible.

Based on the experimental [13] and calculated results, the amorphous phase formation is allowed for shock powers ranging from 4 to 8.2 W (corresponding to 0.4–0.82 W g^{-1} for 10 g $Ni_{10}Zr_7$ powder mass). The ball-milling duration used to obtain the amorphous phases either by the G5 or the G7 planetary ball mill is 48 h [13]. The cumulative kinetic energy is given in Table 1.

A very important point is that an increase in the ball-milling intensity [15] or disc rotation speed for a given vial rotation speed (Fig. 4) does not lead in all cases to the formation of a single amorphous phase. In fact, based on the calculated powers corresponding to the experimental ball-milling conditions reported in Fig. 4, at least three situations may exist.

(1) For low shock powers even an extended time is not sufficient to complete the amorphization process [15].

(2) For medium shock powers (medium ball-milling intensities) a medium ball-milling duration is sufficient to elaborate pure amorphous powders [13] (pure amorphous powders in a large Ni content domain in ref. 15).

(3) For high shock powers, for the same milling duration as for medium shock powers, a mixture of intermetallic crystalline and amorphous phases [13] or intermetallic crystalline phases [15] is obtained.

Eckert *et al.* [15] assume that the temperature during mechanical alloying is a very important parameter of the process. They conclude that a partial crystallization can occur during mechanical alloying at high milling intensities. Thus the crystallization cannot simply be caused by the milling but must be an effect of excess heating during mechanical alloying. To clarify this point

of view, they estimate the peak temperature reached within the powder particles during milling. Based on the procedure proposed by Schwarz and Koch [17], they assume that the particles are deformed by localized shear during collisions between the ball(s) and the vial surfaces. The normal stress developed is

$$\sigma_n = \rho_b V_s V_r \tag{7}$$

where $\rho_b = 8.54$ g cm^{-3} is the density of the steel ball(s), $V_s = 5800$ m s^{-1} is the speed of a longitudinal wave in steel and $V_r = 2.5$, 3.6 and 4.7 m s^{-1} is the relative velocity of the balls for intensities 3, 5 and 7 respectively. The shear process lasts for

$$\Delta t = \frac{2d}{V_s} \tag{8}$$

where $d = 10^{-2}$ m is the diameter of the steel ball(s). The energy flux dissipated on the glide plane is

$$F = \sigma_n V_r \tag{9}$$

The resulting temperature increase ΔT due to the heat flux $F/2$ for time Δt is

$$\Delta T = F\left(\frac{\Delta t}{\pi k_0 \rho_p C_p}\right)^{0.5} \tag{10}$$

where ρ_p and C_p are the powder density and powder specific heat respectively. Based on this procedure, the authors [15] obtained $\Delta T = 80$, 167 and 287 °C for milling intensities 3, 5 and 7 respectively. These values only refer to individual collision processes and must be added to the overall temperature of the milling container, which is about 50, 80 and 120 °C for intensities 3, 5 and 7 respectively. Therefore the total peak temperature of the powder particles can reach 130, 247 and 407 °C. Since an isothermal anneal of the amorphous powders at 400 °C for only 5 min is sufficient to produce partially crystallized materials with a similar X-ray diffraction pattern to that obtained for the $Ni_{70}Zr_{30}$ powder milled for 60 h at intensity 7, the authors [15] conclude that the actual temperature of the individual particles during mechanical alloying can in fact be rather high – at least high enough to cause the crystallization of the formed amorphous particle.

Davis and Koch [18] report on the ball milling of the brittle elements Si and Ge. They show that the ball-milled powders present a neck aspect. The same authors think that localized heating is able to increase the plasticity of the ball-milled powders. Based on the same procedure proposed by Schwarz and Koch [17] and explained above, they estimated the temperature rise in the ball-milled Si and Ge particles. The temperature rises are estimated as $\Delta T = 10.1$ K for the Ge powders and $\Delta T = 6.57$ K for the Si powders. Since it was assumed that the Schwarz procedure is aimed at the bulk temperature rise, the same authors use another procedure aimed at temperature rise estimation on the microstructural scale [19]. This procedure considers the temperature rise as an effect of sliding friction. Based on this method, the temperature rise for the Si–Ge system is estimated as $\Delta t = 4.32$ K. Thus the authors conclude that the observed necking must have another possible explanation. Miller *et al.* [20], using microsecond time-resolved radiometry, observed temperature increases of the order of 400–500 °C upon impacting NaCl crystals.

Hachimoto and Watanabe [21] simulate the energy consumption in a vibratory mill based on the Hertz theory. They assume that the energy consumption increases with increasing ball impact velocity and coefficient of viscosity of the balls, which are assumed to be viscoelastic bodies in the related model simulation. The same authors [21] show that although the coefficient of viscosity has no physical meaning, it has a great influence on the energy consumption. Thus the resulting temperature increase within the powder particles, related to the elastic energy released in the powder, when estimated on the basis of this model, will have no precise value.

In a first analysis we see that there is no agreement between the above-reported estimated temperature rises. All the same, it is important to note that these temperature rises will induce many structural phase transitions. In fact, whatever the method of temperature rise estimation, the estimated temperature rise increases with increasing shock energy. Thus we think that the crystalline phase obtained for high shock power values (Fig. 3) can be the result of a partial crystallization of the formed amorphous phase due to the excess heat.

Bellon and Martin [22, 23] report on the relative stability of non-compound is maintained in a far-from-equilibrium configuration by dynamic external forcing, the steady state properties of the system can no longer be predicted by minimization of the classical thermodynamics potentials (Gibbs or Helmholtz free energy). Thus they assume that the problem will be mapped on to the kinetic Ising model with two competing exchange dynamics: thermally activated jumps and forced atomic jumps. Using master equations, they study the relative stability of several ordered structures under irradiation. They show that under irradiation the ballistic jumps induce transitions which are independent of the state of the system (corresponding to an infinite temperature dynamics), the rate of such jumps being proportional to the replacement cross-section times the irradiation flux. Thus the transition rate is now the sum of two terms, one being the thermal transition rate and the other the ballistic transition rate. The thermal transitions connect only nearest-neighbouring states. Bursts of ballistic jumps connect many states

together. Based on their calculation results, the authors give a dynamic equilibrium phase diagram as a function of the irradiating temperature, the concentration and a reduced parameter which scales the intensity of irradiation as the ratio of the forced to an average thermal A–B pair permutation frequency. Based on these above results, the end product was assumed to be a result of competition between thermally activated jumps (classical diffusion) and forced atomic jumps (ballistic effect).

Schwarz and Koch [17] suggest that the critical defect concentration introduced by mechanical alloying will promote spontaneous transformation to the amorphous state. At this defect concentration $G_c + \Delta G_d > G_a$, where G_c is the free energy of the crystalline phase, ΔG_d is the increase in free energy due to the defects introduced by MA and G_a is the free energy of the amorphous phase. The experimental observations [27] are consistent with this concept. They show that intermetallic compounds with narrow homogeneity ranges tend to become amorphous during irradiation, while compounds with wide solubilities tend to remain crystalline. This difference was attributed [27] to a smaller increase in ΔG_d for a given defect density for the latter alloys, reflected by their ability to exist away from perfect stoichiometry.

This mechanism may explain the amorphization by MA when starting from crystalline powders of intermetallics. It does not seem adequate, however, to explain the amorphization by MA when starting from a mixture of pure crystalline powders. Schwarz *et al.* [28] suggest that the amorphization by mechanical alloying when starting from a mixture of pure crystalline powders occurs by solid state interdiffusion reaction near clean boundaries between polycrystalline powders. The mixing is assisted by the excess point and lattice defects created by plastic deformations.

Martin and Gaffet [29] assume that the frequency of forced jumps (in connection with the forced jumps induced by irradiation) scales with the shock power injected mechanically into the material. Indeed, most of the shock power is dissipated into heat; a small fraction (about 10%) is injected into the lattice in the form of vacancies or antisite defects [30]. Following the above ideas, the authors [13, 31–33] do a systematic search for milling conditions which promote amorphization in an $Ni_{10}Zr_7$ compound. A narrow domain of amorphization is clearly visible. The authors [29] assume that amorphization proceeds below a certain power input and above a minimum energy per impact. If the power is too high, too much heating may occur. The minimum energy per impact requirement may be imposed by the yield stress of the particles [26].

Figure 3 illustrates the dynamic end product phase diagram which is mapped into three regions as a function of the shock power, the first corresponding to the formation of a mixture of amorphous and crystalline phases reported for low power values, the second corresponding to the formation of pure amorphous powders reported for medium power values and, finally, the third corresponding to the formation of a mixture of amorphous and crystalline phases reported for high power values.

Thus we assume that for low shock power values the increase in the free energy of the crystalline powders due to the stored elastic energy (or the shock power) as defects and antisites is not too high to promote the formation of only a pure amorphous phase and the input crystalline powders are able to remain crystalline even at such a shock power. For the medium shock power level the increase in free energy due to the stored elastic energy is such that $G_c + \Delta G_d > G_a$, where G_c is the free energy of the crystalline phase, ΔG_d is the increase in free energy due to the defects introduced by MA and G_a is the free energy of the amorphous phase. Thus only a pure amorphous phase is able to be formed. For the high shock power level we have, as with the low power level, the formation of a mixture of crystalline and amorphous phases. We assume that a partial crystallization of the formed amorphous phase occurs owing to the excess localized heating. Thus we assume that the amorphization proceeds above a minimum power input and below a certain maximum power input.

Chen *et al.* [24] report some results documented in the material literature concerning the kinetic energy, shock frequency and shock power for three common devices: the Attritor ball mill, the planetary ball mill (Fritsch "Pulverisette P5") and the vibratory grinder (*e.g.* SPEX Shaker mill). Table 3 gives the documented [24] and calculated values (for the G5 and G7 planetary ball mills) of the kinetic energy, shock frequency and shock power.

Based on Table 3, the G5 shock power domain overlaps all the other devices' shock power domains. Moreover, it was reported by Martin and Gaffet [29] that the ball-milling power input domain overlaps some typical mechanical straining or irradiating power input domains. Thus we assume that the G5 planetary ball mill is able to induce the same phase transitions that can be induced by all the other devices.

4. Conclusions

Based on a mathematical treatment of the process taking place in a planetary ball mill and experimental results concerning the ball-milled end product of the $Ni_{10}Zr_7$ compound, we prove that neither the shock energy nor the shock frequency separately governs the

TABLE 3. Documented and calculated values of kinetic energy, shock frequency and shock power for various ball mills

	Attritor mill	Vibratory mills		Planetary ball mills		
		Pulv. O	SPEX	Pulv. P5	G7	G5
Velocity of balls ($m\ s^{-1}$)	0–0.8 [12]	0.14–0.24 [21]	<3.9 [12]	2.5–4 [14]	0.24–6.58 [a]	0.28–11.24 [a]
Kinetic energy (10^{-3} J per hit)	<10	3–30	<120	10–400	0.4–303.2 [a]	0.53–884 [a]
Shock frequency (Hz)	>1000 [22]	15–50 [21]	200 [20]	~100 [22]	5.0–92.4 [a]	4.5–90.7 [a]
Power ($W\ g^{-1}$ per ball)	<0.001	0.005–0.14	<0.24	0.01–0.8	0–0.56 [a]	0–1.604 [a]

[a]This work.

ball-milled end product, but that only the injected shock power is responsible for the ball-milled end product.

Based on our calculation results and experimental results [13], a dynamic end product phase diagram (Fig. 3) is mapped into three regions as a function of the shock power, the first corresponding to the formation of a mixture of amorphous and crystalline phases reported for low power values, the second corresponding to the formation of pure amorphous powders reported for medium power values and the third corresponding to the formation of a mixture of amorphous and crystalline phases corresponding to high power values.

Acknowledgments

This work has been performed using the CECM/CNRS (Vitry/Seine) and IMN/CNRS (Nantes) computers. We thank O. Pellegrino, J.M. Larre and J.M. Barbet for their help.

References

1 E. Gaffet, *Mater. Sci. Eng. A, 136* (1991) 161–169; P.H. Shingu (ed.), *Proc. Int. Symp. on Mechanical Alloying, Kyoto, May 1991,* Trans Tech, Zürich - CH, 1992.
2 E. Gaffet and M. Harmelin, *J. Less-Common Met., 157* (1990) 201–222.
3 M. Sherif El-Eskandarany, K. Aoki, H. Itoh and K. Suzuki, *J. Less-Common Met., 169* (1991) 235–244.
4 F. Bordeaux and A.R. Yavari, *J. Appl. Phys., 67*(5) (1990) 2385.
5 A. Calka, A.P. Pogany, R.A. Shanks and H. Engelman, *Mater. Sci. Eng. A, 128* (1990) 107–112.
6 T.J. Tianen and R.B. Schwarz, *J. Less-Common Met., 140* (1988) 99.
7 M.S. Kim and C.C. Koch, *J. Appl. Phys., 62* (1987) 3450.
8 C. Suryanarayana and F.H. Froes, *Nanostruct. Mater., 1* (1992) 191–196.
9 E. Gaffet, C. Louison, M. Harmelin and F. Faudot, *Mater. Sci. Eng. A, 134* (1991) 1380–1384.
10 M. Abdellaoui, T. Barradi and E. Gaffet, *J. Alloys Comp., 198* (1993) 155–164.
11 N. Burgio, A. Iasonna, M. Magini, S. Martelli and F. Padella, *Nuovo Cimento D, 13* (1991) 459.
12 D.R. Maurice and T.H. Courtney, *Metall. Trans. A, 21* (1990) 289–303.
13 E. Gaffet and L. Yousfi, *Mater. Sci. Forum, 88–90* (1992) 51–58.
14 Y. Chen, R. Le Hazif and G. Martin, *Mater. Sci. Forum, 88–90* (1992) 35–42.
15 J. Eckert, L. Schultz, E. Hellstern and K. Urban, *J. Appl. Phys., 64*(6) (1988) 3224.
16 H.J. Fecht, *Nanostruct. Mater., 1* (1992) 125–130.
17 R.B. Schwarz and C.C. Koch, *Appl. Phys. Lett., 49* (1986) 146.
18 R.M. Davis and C.C. Koch, *Scr. Metall., 21* (1987) 305–310.
19 H.S. Carslaw and J.C. Jaeger, *Heat Conduction in Solids,* Oxford University Press, New York, 1959, p. 225.
20 P.J. Miller, C.S. Coffey and V.F. Devost, *J. Appl. Phys., 59*(3) (1986) 913.
21 H. Hachimoto and R. Watanabe, *Mater. Trans. JIM, 31*(3) (1990) 219–224.
22 P. Bellon and G. Martin in A.R. Yavari (ed.), *Proc. Eur. Workshop on Ordering and Disordering in Alloys, Grenoble 1991,* Elsevier, Amsterdam, 1992, pp. 172–181.
23 P. Bellon and G. Martin, *Solid State Phenom., 3–4* (1988) 109–124.
24 Y. Chen, R. Le Hazif and G. Martin, *Solid State Phenom., 23–24* (1992) 271–284.
25 R.M. Davies, B. Mcdermott and C.C. Koch, *Metall. Trans., A, 19* (1988) 2867.
26 B.N. Babich and V.A. Djatlenko, in F.H. Froes and J.J. DeBabardillo (eds.), *Structural Applications of MA, 1989,* ASM International, Materials Park, OH, 1990, p. 287.
27 J.L. Brimhall, H.E. Kissinger and L.A. Charlot, *Radiat. Effects, 77* (1983) 237.
28 R.B. Schwarz, R.R. Petrich and C.K. Saw, *J. Non-Cryst. Solids, 76* (1985) 281.
29 G. Martin and E. Gaffet, *J. Phys. (Paris), Colloq. C4, 51* (Suppl. 14) (1990) 71–77.

30 H. Mecking and Y. Estrin, *Scr. Metall., 14* (1980) 815.
31 E. Gaffet, *Mater. Sci. Eng. A, 119* (1989) 185–197.
32 E. Gaffet, *Mater. Sci. Eng. A, 132* (1991) 181–193.
33 E. Gaffet, *Mater. Sci. Eng. A, 135* (1991) 291–293.
34 M. Abdellaoui and E. Gaffet, *Acta Metall. Mater.*, submitted for publication.

Appendix: Mathematical treatment of the process taking place in a planetary ball mill

Here we give the results of the study of the ball motion in the vial during one cycle. Application of the fundamental dynamic principle gives the detachment condition which allows the calculation of the detachment position and detachment velocity. These latter parameters are used to calculate the motion of the ball from a detachment event until a collision event. The collision velocity gives the kinetic energy released from the ball to the powders. The time between two collision events or two detachment events gives the shock frequency.

Figure A1 shows the ball position "M" at a "t" event, where R (m) is the disc radius, r (m) is the vial radius, r_b (m) is the ball radius, m (kg) is the ball mass, M is a material point representing the ball position in the vial, $\theta = \Omega t$ is the disc rotation angle, with $\vec{\Omega} = \Omega\vec{K}$ the angular disc rotation speed, $\alpha = -wt$ is the vial rotation angle, with $w = -w\vec{K}$ the angular vial rotation speed, $U_\rho // \vec{R}$, $\vec{U}_\theta \perp \vec{U}_\rho$, $\vec{u}_\rho // \vec{r}$ and $\vec{u}_\alpha \perp \vec{u}_\rho$.

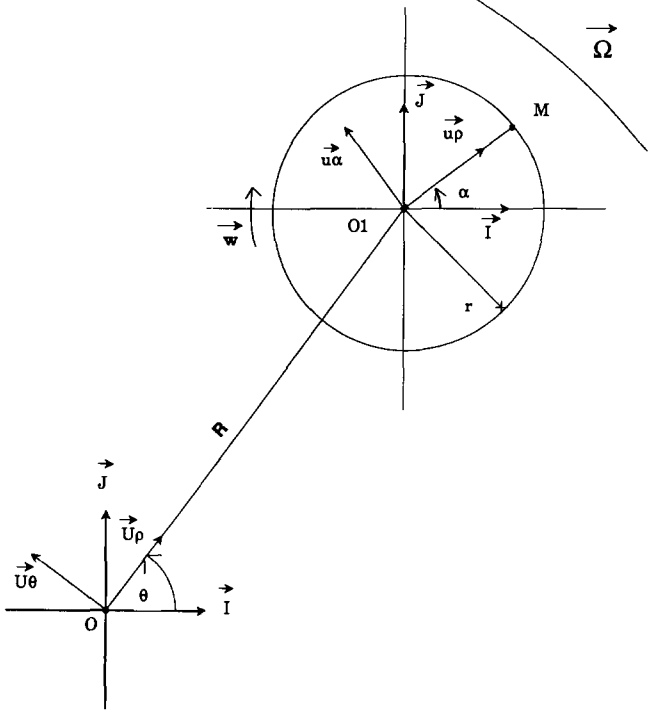

Fig. A1. Geometry of the disc and one vial seen from the top. The various vectors and angles are explained in the text.

The amplitudes of the absolute velocity and absolute acceleration of the ball before a detachment event are respectively [34]

$$\|\vec{V}_a\|^2 = (R\Omega)^2 + (rw)^2 - 2Rr\Omega w\cos(\theta-\alpha) \quad \text{(A1)}$$

$$\|\gamma_a\|^2 = (R\Omega^2)^2 + (rw^2)^2 + 2Rr\Omega^2 w^2\cos(\theta-\alpha) \quad \text{(A2)}$$

Based on the fundamental dynamic principle, in a reference fixed to the ball, the detachment condition of the ball from the inner vial surface is $\cos(\alpha-\theta) = -rw^2/R\Omega^2$. For more details see ref. 34. Thus the amplitudes of the absolute velocity and absolute acceleration of the ball at a detachment event, taking into account the ball radius, are respectively

$$\|\vec{V}_d\|^2 = (R\Omega)^2 + (r-r_b)^2 w^2\left(1+\frac{2w}{\Omega}\right) \quad \text{(A3)}$$

$$\|\vec{\gamma}_d\|^2 = (R\Omega^2)^2 - [(r-r_b)w^2]^2 \quad \text{(A4)}$$

To obtain the time between detachment and collision events, a numerical solution using computer facilities is adopted. Figure A2 shows the ball motion from a detachment event up to a collision event, where (θ_d, α_d) and (θ_c, α_c) are the values of the disc and vial angular positions at the detachment and collision events respectively, $\vec{V}_d$ and $\vec{V}_c$ are the detachment and collision velocities respectively, M_d and M_c are the ball positions at the detachment and collision events respectively and ($\vec{u}_{\rho d}$, $\vec{u}_{\alpha d}$) and ($\vec{u}_{\rho c}$, $\vec{u}_{\alpha c}$) are the vectors defining the cylindrical referentials at the detachment and collision events respectively. For the numerical calculations, to have an easy and clear geometrical formulation and further simplification of the parameter calculations, we assume that the θ_d value corresponding to the detachment event is equal to $\pi/2$. If we give another value to the θ_d angle, this will cause a change in the value of the α_d angle corresponding to the detachment event, but the calculation result will remain unchanged.

The first collision event occurs when the following condition is fulfilled: $x = OP_x$ and $y = OP_y$, with x and y the ball coordinates after the detachment event and OP_x and OP_y the coordinates of a point of the inner vial surface (for the collision event OP_x and OP_y represent the coordinates of the M_c point (Fig. A2)). The calculation details of x, y, OP_x and OP_y are reported in ref. 34. A numerical solution of this condition is obtained using the computer facilities. The numerical calculation consists of

(1) incrementation of the time value by a time step interval Δt (ms),

(2) calculation of the θ angle value ($q = \pi/2 + \omega t$),

(3) variation of the α angle value from 0 up to -2π by incrementing its value by a negative angle step interval $\Delta\alpha$ of $-0.01°$ (the $\Delta\alpha$ value is negative to have a vial rotation sense opposite to the disc one), and finally

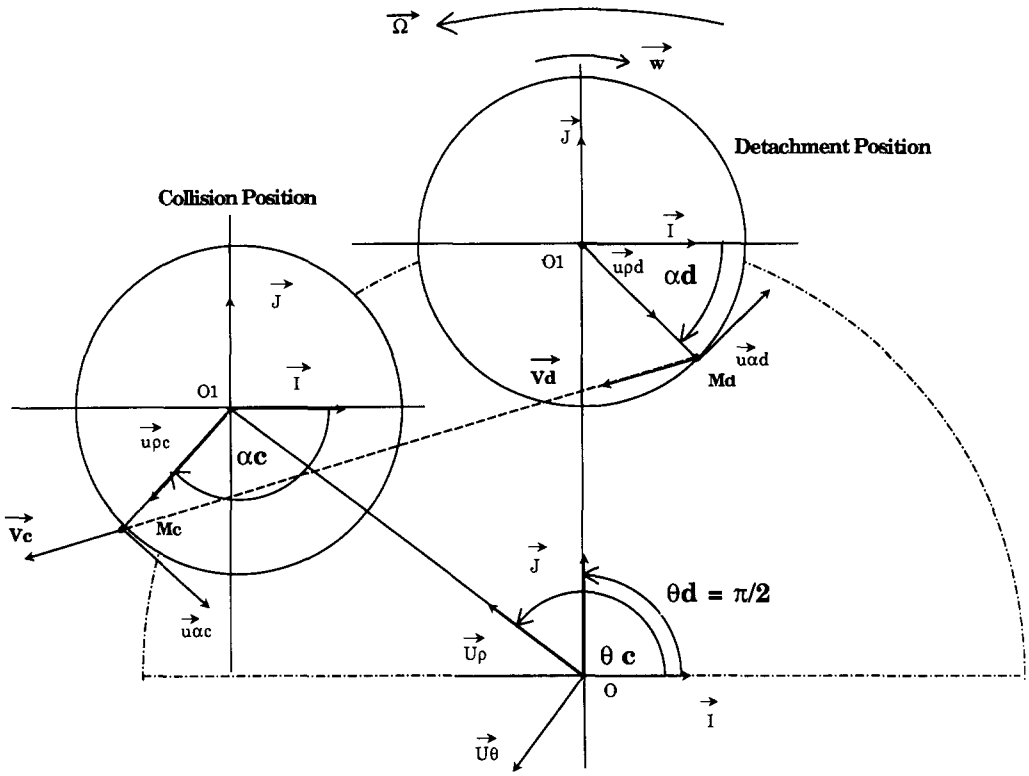

Fig. A2. Absolute velocity and ball position at detachment and collision events. The various vectors are explained in the text.

(4) calculation of the OP_x, OP_y, x and y values.

If the condition $x = OP_x$ and $y = OP_y$ is fulfilled, we have the first collision point coordinate values (x and y) along the X and Y axes as well as the time t needed between the first detachment event and the first collision event.

The ball is assumed to have a linear uniform motion after its detachment. Thus the collision velocity will be equal to the detachment velocity and the kinetic energy E_k is given as

$$E_k = \tfrac{1}{2}m\|\vec{V}_c\|^2 = \tfrac{1}{2}m\|\vec{V}_d\|^2 \quad \text{(A5)}$$

The shock frequency f is the number of collisions per second. The cycle period is the sum of two periods T_1 and T_2, with T_1 the period of time needed by the ball to go from the detachment point up to the collision point (equal to the t period such that the condition $x = OP_x$ and $y = OP_y$ is fulfilled) and T_2 the period of time needed between the first collision event and the second detachment event. Thus the shock frequency final expression is

$$f = \frac{1}{T} = \frac{1}{T_1 + T_2} \quad \text{(A6)}$$

For more details on the frequency calculations see ref. 34.

When operating with a number of balls greater than one, the shock frequency is equal to the product of one ball frequency as calculated above and the number of balls corrected by a factor of 1 or less. This has been studied by Burgio *et al.* [11].

The power released by the ball to the powders is the product of the shock frequency and kinetic energy. It is given by the expression

$$P = fE_k \quad \text{(A7)}$$

To get the total cumulative kinetic energy E_{kc} released from the ball to the powders during a given ball-milling duration "BMD", we multiply the shock power (eqn. (7)) by the value of the ball-milling duration, *i.e.*

$$E_{kc} = P \times \text{"BMD"} \quad \text{(A8)}$$